X-ray-spectroscopy analysis of electron-cyclotron-resonance ion-source plasmas

J. P. Santos,[1] A. M. Costa,[2] J. P. Marques,[2] M. C. Martins,[1] P. Indelicato,[3] and F. Parente[1]

[1]*Centro de Física Atómica, CFA, Departamento de Física, Faculdade de Ciências e Tecnologia, FCT, Universidade Nova de Lisboa, P-2829-516 Caparica, Portugal*

[2]*Centro de Física Atómica, CFA, Departamento de Física, Faculdade de Ciências, FCUL, Universidade de Lisboa, Campo Grande, P-1749-016 Lisboa, Portugal*

[3]*Laboratoire Kastler Brossel, École Normale Supérieure, CNRS, Université P. et M. Curie – Paris 6, Case 74; 4, place Jussieu, F-75252 Paris CEDEX 05, France*

Analysis of x-ray spectra emitted by highly charged ions in an electron-cyclotron-resonance ion source (ECRIS) may be used as a tool to estimate the charge-state distribution (CSD) in the source plasma. For that purpose, knowledge of the electron energy distribution in the plasma, as well as the most important processes leading to the creation and de-excitation of ionic excited states are needed. In this work we present a method to estimate the ion CSD in an ECRIS through the analysis of the x-ray spectra emitted by the plasma. The method is applied to the analysis of a sulfur ECRIS plasma.

PACS number(s): 32.70.−n, 32.70.Fw

I. INTRODUCTION

Electron-cyclotron-resonance ion sources (ECRIS) are widely used to provide low to medium-high charge-state ions for heavy-ion accelerators as well as a standalone device to provide low-energy ion beams. Their plasmas are also more and more used as powerful sources of radiation, whether to provide vacuum-ultraviolet radiation sources [1] or intense sources of highly charged ion x rays [2,3]. The radiation emitted by the ions in the plasma can be used for plasma diagnostic [4,5], for spectrometer characterization [6], and to provide accurate transition energies of highly charged ions.

ECRIS are small mirror machines [7]. A magnetic bottle is created using either permanent magnets, or normal or superconducting coils, to confine longitudinally an electron gas. Transverse confinement is obtained by means of a multipole field, most frequently an hexapole, usually made out of permanent magnets, although several devices such as the VENUS in Berkeley [8] and SERSE in Catania [9,10] use superconduting coils. Other devices, such as the ECR ion trap (ECRIT) at the Paul Scherrer Institute (PSI) [11], use a combined superconducting coils magnetic bottle and a permanent magnet hexapole [11]. The electron plasma is heated by a microwave field: The electrons have a spiral motion around the field lines with the cyclotron frequency (Larmor frequency), and are resonantly accelerated when they pass the resonance zone, where their cyclotron frequency is equal to the frequency of the injected microwaves.

In the present paper, we deal with the line spectrum from a sulfur plasma, created at the PSI ECRIT [11]. Theoretical and experimental work on electrons of ECRIS plasmas show that the electron velocity distribution function is non-Maxwellian, although it can be schematically represented by several Maxwellian distributions for the cold, warm, and hot electrons [12], or by a Maxwellian distribution for the cold, or thermal, electrons and a non-Maxwellian distribution for the hot electrons [13]. These electrons may then excite and ionize the injected atoms or molecules, which will form a plasma. The ions may subsequently be extracted from the plasma and/or the emitted radiation can be detected.

Although electrons in ECRIS are energetic, ions are rather cold. Owing to the large ratio of ion-to-electron masses and to the large average electron energy, the electron-ion collisional heating cannot be very efficient and the electron-ion energy equipartition occurs on a timescale (in the range of a few seconds) much larger than that of the ion confinement (about three orders of magnitude) [14]. Furthermore, the energetic ions in the space charge of the electron shallow potential, of the order of a few eV [15], will escape from this region.

The ion-ion collision frequency is large enough so that the energy equipartition terms between ions rapidly become negligible. Ions are therefore Maxwellian with the same temperature, regardless of ion charge states or ion species.

One of the main problems of ECRIS plasma diagnostics is the determination of the ion charge-state distribution (CSD) inside the plasma. Although one could try to deduce the CSD from extracted ion beam currents, this is not a very reliable method. As the extraction is optimized for a particular charge state and the ions are extracted from the plasma edges, the current would not exactly reflect the CSD inside the plasma.

Alternatively, the CSD inside the plasma may be obtained nonintrusively through the analysis of high-resolution x-ray spectra emitted by the ECRIS [16–20]. In fact, ECRIS are characterized, among other properties, by their capacity to produce x-ray emission, including bremsstrahlung and characteristic lines, which can thus be used for plasma diagnostics. Similar processes for optical plasma diagnostics were reviewed in the work of Boffard *et al.* [21].

In 2000, Douysset *et al.* [4] estimated the ionic density of each charge state in an ECRIS plasma through the measurement of the intensity of the emitted $K\alpha$ lines. In the same year, Küchler *et al.* [20] proposed a method to predict the x-ray spectrum, taking into account the main atomic processes, in which they solve numerically the balance

equations for the ion densities and the electron energy distribution. The modeled spectrum is fitted by adjusting the parameters of the simulation, namely the ion CSD. This method considers a single Maxwellian distribution for the electrons, uses an expression derived for neutral atoms to calculate the electron impact excitation of ions, and assumes that the fluorescence yield is independent of the charge state, which is a crude approximation for the highest ion charge states.

In 2001, the present authors [22] performed a detailed analysis of *K* x-ray spectra emitted by Ar ions in an ECRIS plasma as reported in Ref. [4]. This showed that a complete analysis of these spectra calls for a careful examination of all excitation and ionization processes that lead to the excited states of the different ionic species whose decay will yield the detected lines. In that work, the relevant atomic parameters were calculated for each charge state but a single average energy for the electrons in the plasma was used.

In the present work, we present a more precise method to estimate the ion CSD in an ECRIS through the analysis of the x-ray spectra emitted by the plasma, that uses a more realistic electron energy distribution and takes into account the electron-impact triple ionization process.

This article is organized as follows. In Sec. II, we describe the relevant atomic processes of creation of highly excited states in an ECRIS plasma and the methods used to compute the corresponding cross sections. In Sec. III, the electron energy distribution in the plasma is discussed. In Sec. IV, we present the calculation of line intensities and, in Sec. V, we review the results obtained for sulfur and discuss the limitations of the method.

II. PROCESSES OF CREATION AND DECAY OF HIGHLY EXCITED STATES IN AN ECRIS

The methodology used to estimate the ion CSD in this work includes the following steps:

(1) The spectrum of characteristic x rays from ions inside the plasma is measured.

(2) The excited states that produce the x-ray spectrum are identified.

(3) The main processes leading to these excited states, from the ground configurations, are found and the corresponding cross sections are calculated, using a physically justified electron distribution function.

(4) Radiative and radiationless transition energies and probabilities are calculated for the identified excited states.

(5) From the comparison of the peak intensities in theoretical and experimental spectra we arrive at the ion charge-state density ratios.

In the ECRIS plasma we can assume that the ions are in their ground configurations, since the lifetimes of the excited configurations are orders of magnitude lower than the collision times for *K* excitation or *K*, *KL*, or *KLL* ionization. There are, however, a few metastable states, like the $1s^2 2s 2p\,^3P_0$ state in Be-like ions, which could live long enough (it can only decay by a very forbidden E1M1 two-photon transition) to be considered as alternative ground states. For isotopes having a nonzero nuclear magnetic moment, such states are subject

to hyperfine quenching, which can reduce their quasi-infinite lifetime dramatically. In the case of sulfur, however, the most abundant isotopes, ^{32}S (94.9%) and ^{34}S (4.3%), have zero magnetic moments and even for the other isotopes their lifetime remains very long (a few seconds) [23,24]. The situation would be the same for several other charge states like Mg-like ions [25,26]. Yet we could not find any spectroscopic indications that such long-lived states do contribute to the observed spectra.

X-ray line emission from ECR plasmas is related to various atomic processes: electronic inner-shell ionization and excitation, dielectronic recombination, charge exchange reactions, radiative recombination, and radiative and radiationless decays. For highly charged ions, dielectronic recombination, charge exchange, and radiative recombination rates are low compared to the dominant processes, which are inner-shell ionizations, and radiative and radiationless decays [4].

A. Electron-impact excitation

Interpretation of plasma spectroscopic spectra requires knowledge of many values of the electron-impact excitation cross sections for atoms and ions. Many cross-section values have been already calculated, or determined experimentally, for some systems and for some intervals of incident electron energy and, therefore, can be found in the literature and in atomic databases [27,28]. However, published cross sections are often insufficient for detailed simulation of experiments, since they do not cover the entire energy range required for calculation of excitation rates, and/or the particular ions.

Estimates of electron-impact excitation cross sections are frequently provided by the Fisher *et al.* expression [29], which is based on the van Regemorter expression for bound-bound electron excitation [30]. Nevertheless, the use of this formula is questionable for ions, because it was derived for neutral atoms and also because it only takes into account electric dipole transitions.

To overcome this limitation, the excitation cross sections should be calculated by computer codes designed for this purpose (see, e.g., Ref. [31] for a list of software for atomic physics).

To compute the electron-impact excitation cross sections we used the multiconfiguration Dirac-Fock and general matrix elements (MDFGME) computer code of Desclaux and Indelicato [32–34], because it calculates accurately not only the excitation cross sections, but also the other atomic parameters needed for modeling the x-ray spectra from an ECRIS plasma, namely transition energies and radiative and radiationless transition probabilities. This code calculates the excitation cross sections by using the first Born approximation with multiconfiguration Dirac-Fock (MCDF) wave functions for the atom and a Dirac wave function for the free electron [35].

B. Electron-impact ionization

The quantitative quantum-mechanical description of the ionization cross sections by electron impact of multielectron correlated systems is a problem with a high degree of complexity, even for electron-impact single ionization [36]. During the past two decades, several powerful computer-intensive

theoretical methods to calculate electron-impact ionization cross sections have been developed [37–43]. Some of these methods provide remarkable agreement with experiment for simple systems like hydrogen, helium, and sodium. The price to pay for this agreement is the long computing time required even with the most powerful computers and, more importantly, limited applicability to targets with complex valence shell structures and heavy atoms. However, for many applications like those in plasmas or, in particular, in ECRIS plasmas, there is a need to obtain ionization cross sections in a closed analytical form using relatively simple formulas. Such formulas should be based upon a quantum-mechanical treatment with a suitable description of the asymptotic high-energy behavior of the cross sections so that they can be used in high energetic electrons.

1. Electron-impact single ionization

Many researchers looked at different times for electron-impact single ionization empirical or semiempirical expressions, which would fit the experimental data. We can cite, for example, the expressions developed by Lotz [44], Deutsch *et al.* [45], Casnati *et al.* [46], and Quarles [47].

Kim and Rudd [48] proposed the binary-encounter-Bethe (BEB) model, which was used to calculate total ionization cross sections of neutral atoms and molecules with great success [27,49,50] for nonrelativistic incident electron energies.

When the incident electron kinetic energy E exceeds about 20 keV, as in inner-shell ionization of heavy atoms by fast electrons or stripping of fast ion projectiles used in heavy-ion fusion, one needs to take the relativistic interaction between the incident and target electrons into account. Recently, Kim *et al.* [51], obtained an expression, referred to as RBEB, which is an extension of the nonrelativistic BEB formula to relativistic incident electrons. This expression requires only three orbital constants besides E: the kinetic energy of the ejected electron U, the orbital binding energy B, and the electron occupation number N for the pertinent shell.

The RBEB expression has provided accurate results, even at energies close to the ionization threshold [51,52], and reads

$$\sigma_{RBEB} = \frac{4\pi a_0^2 \alpha^4 N}{(\beta_t^2 + \beta_u^2 + \beta_b^2)2b'} \left\{ \frac{1}{2} \left[\ln\left(\frac{\beta_t^2}{1-,\beta_t^2} \right) - \beta_t^2 - \ln(2b') \right] \right.$$
$$\times \left(1 - \frac{1}{t^2} \right) + 1 - \frac{1}{t} - \frac{\ln t}{t+1} \frac{1+2t'}{(1+t'/2)^2}$$
$$\left. + \frac{b'^2}{(1+t'/2)^2} \frac{t-1}{2} \right\}, \tag{1}$$

where

$$\beta_t = v_t/c, \quad \beta_t^2 = 1 - \frac{1}{(1+t')^2},$$
$$t = E/B, \quad t' = E/mc^2, \tag{2}$$

$$\beta_b = v_b/c, \quad \beta_b^2 = 1 - \frac{1}{(1+b')^2}, \quad b' = B/mc^2, \tag{3}$$

$$\beta_u = v_u/c, \quad \beta_u^2 = 1 - \frac{1}{(1+u')^2}, \quad u' = U/mc^2. \tag{4}$$

Here, v_t is the speed of an electron with kinetic energy E, v_b is the speed of an electron with kinetic energy B, v_u is the speed
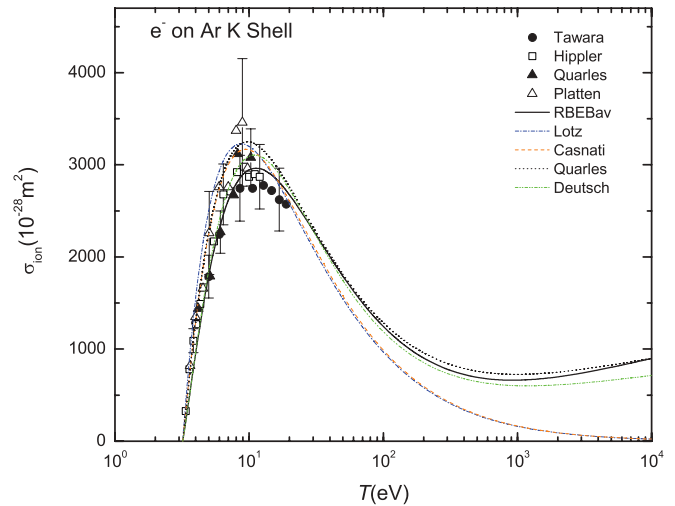

FIG. 1. (Color online) *K*-shell ionization cross section of Ar. Solid circles, experimental data by Tawara *et al.* [85]; squares, experimental data by Hippler *et al.* [86]; solid upright triangles, experimental data by Quarles and Semaan [87]; upright triangles, experimental data by Platten *et al.* [88]; thick solid curve, present RBEBav cross section Eq. (5); dot-dashed curve, nonrelativistic empirical formula by Lotz [44,89]; dashed curve, nonrelativistic empirical formula by Casnati *et al.* [46]; dotted curve, the Casnati cross section with relativistic corrections by Quarles [47]; dot-dot-dashed curve, relativistic semiempirical formula by Deutsch *et al.* [45].

of an electron with kinetic energy U, α is the fine-structure constant, a_0 is the Bohr radius, m is the electron mass, and c is the speed of light.

For single ionization of tightly bound inner shells, which are subject to strong nuclear attraction, and for ions whose net charge is +3 or higher, Kim *et al.* [51] proposed the averaged RBEB expression,

$$\sigma_{RBEBav} = \frac{1}{2} \left(1 + \frac{\beta_t^2 + \beta_u^2 + \beta_b^2}{\beta_t^2} \right) \times [\text{RHS of Eq. (1)}], \tag{5}$$

where RHS stands for the right-hand side of the equation.

In Figs. 1 and 2, we compare the RBEBav [Eq. (5)] cross sections for *K*-shell ionization of Ar ($Z = 18$) and Se ($Z = 34$) to available experimental data, the nonrelativistic empirical cross sections from the formula of Lotz [44], the nonrelativistic empirical cross sections from the formula of Casnati *et al.* [46], the relativistic version of the formula of Casnati *et al.* as modified by Quarles [47], and the nonrelativistic semiempirical cross sections from the formula of Deutsch *et al.* [45]. We observe that the RBEBav cross sections tend to agree better with the experimental data in general. It should be noticed that the experimental data of Berenyi *et al.* [53] for the selenium atom confirm the relativistic cross sections behavior at 200 keV < T < 800 keV, and therefore the need to use a relativistic expression, as the RBEBav one.

In our opinion, the RBEBav expression (5) is ideally suited for modeling ionizing events that cover incident electron energies from the threshold to relativistic values, such as those in the ECRIS plasma, because it provides accurate
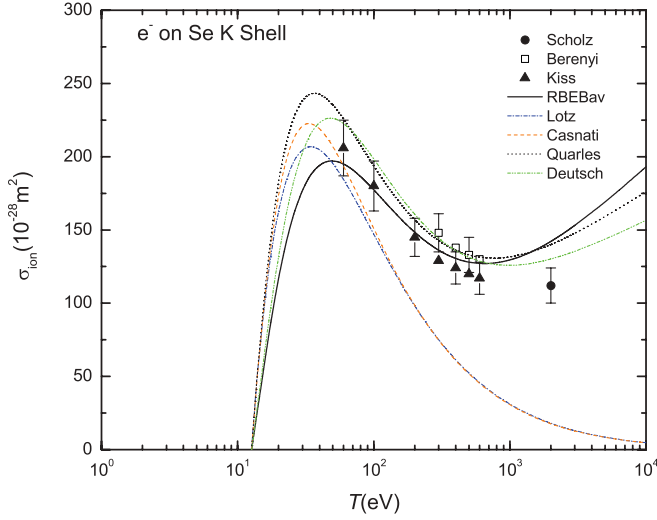
FIG. 2. (Color online) *K*-shell ionization cross section of Ar. Solid circles, experimental data by Scholz *et al.* [90]; squares, experimental data by Berenyi *et al.* [53]; solid upright triangles, experimental data by Kiss *et al.* [91]; thick solid curve, present RBEBav cross section Eq. (5); dot-dashed curve, nonrelativistic empirical formula by Lotz [44,89]; dashed curve, nonrelativistic empirical formula by Casnati *et al.* [46]; dotted curve, the Casnati cross section with relativistic corrections by Quarles [47]; dot-dot-dashed curve, relativistic semiempirical formula by Deutsch *et al.* [45].

cross-section values, requires minimal input data for the target, and does not require adjustable empirical parameters.

2. Electron-impact double and triple ionization

From the analysis of x-ray spectra emitted by ECRIS plasmas, we found that, in order to explain their main features, double and triple ionization processes have to be taken in account.

Thus, in this method we include the double *KL*-ionization and triple *KLL*-ionization processes from the ions ground configurations. For the calculation of these cross sections we used the semiempirical formula developed by Shevelko and Tawara [54], with the fitting parameters proposed by Bélenger *et al.* [55], which, to our knowledge, is the only analytical expression that provides cross sections for multiple ionization processes. This expression, in cm^2 units, reads

$$\sigma_n = \frac{a(n)N^{b(n)}}{(I_n/\mathrm{Ry})^2}\left(\frac{u}{u+1}\right)^c \frac{\ln(u+1)}{u+1}10^{-18}, \qquad (6)$$

with

$$u = \frac{E}{I_n} - 1, \qquad (7)$$

where E is the incident electron energy in eV, I_n is the ionization energy in eV required to remove the *KL*, or *KLL*, electrons from the target, N is the total number of target electrons, $1\,\mathrm{Ry} = 13.6\,\mathrm{eV}$, and $c = 1$ for neutral atoms and $c = 0.75$ for ions. The fitting parameters a and b were evaluated from experimental data [55], and they are $a(2) = 14.0$ and $b(2) = 1.08$ for the removal of two electrons, and $a(3) = 6.30$ and $b(3) = 1.20$ for the removal of three electrons. It should be

noticed that this expression was developed for the ionization of the outermost electrons.

C. Transition energies and probabilities

For a correct identification of the peaks in high-resolution x-ray spectra (∼0.3 eV), the importance of knowledge of precise transition energy values cannot be overemphasized. Electrons in highly charged ions, especially in inner shells, are, in general, highly relativistic, so a relativistic calculation is in order. The correlation contribution to transition energies is very important in few electron ions, which calls for the use of multiconfiguration or configuration-interaction approaches. Finally, quantum-electrodynamics effects (QED) must, in general, be taken into account. The details of the contributions included in the present work are given in Sec. V later.

For this purpose, we took the following steps:

(1) Precise calculation of the energy values for the initial and final levels of the pertinent radiative and radiationless transitions.

(2) Calculation of the transition probability values for all considered transitions.

(3) Evaluation of fluorescence yield values.

III. DISTRIBUTION OF ELECTRON ENERGIES IN THE PLASMA

Electrons in an ECRIS plasma are far from thermodynamical equilibrium. The electron distribution function $f(E)$ is strongly non-Maxwellian and can be represented by two populations [13]: a cold one (energies up to 10 keV) and a hot one (energies of several tens of keV); the latter is well confined inside a closed egg-shaped surface centered around the source main axis. Barué *et al.* [13] and Gumberidze *et al.* [5] studied experimentally the energy distribution of the hot electrons observing bremsstrahlung and electron cyclotron emission.

The cold electrons distribution can be considered approximately as Maxwellian, whereas the hot electrons distribution is non-Maxwellian. Following Pras *et al.* [56], we write the global electron distribution $f(E)$ as a linear combination of the Maxwellian, $f_{\mathrm{Mw}}(E)$, and the non-Maxwellian, $f_{\mathrm{NMw}}(E)$, electron distributions.

If N_e, $v(E)$ and $\sigma(E)$ are the electron density, the electron velocity and the cross section for a given process, respectively, at a specific electron energy E, then the quantity $\langle N_e\sigma v\rangle$ gives the rate of the number of events related to a process (excitation or ionization), averaged over the electron distribution energy, and is defined by

$$\langle N_e\sigma v\rangle = N_e\int_{E_{\min}}^{\infty}v(E)\sigma(E)f(E)\,dE$$
$$= N_e\int_{E_{\min}}^{\infty}v(E)\sigma(E)$$
$$\times[(1-x)f_{\mathrm{Mw}}(E) + xf_{\mathrm{NMw}}(E)]\,dE, \qquad (8)$$

where x is a mixing coefficient. In order to evaluate the integrals, the cross sections for all the processes considered have

to be calculated for several energy values from threshold, E_{min}, to infinity, which is an impossible task when the cross sections are not given by simple analytical expressions. Fortunately, the mathematical form of the electron distributions used here is well suited for the use of the Gauss-Laguerre integration method. Using this method, only a small number (7 to 20) of cross-section values needs to be calculated for each process, each ion, and each temperature value.

In order to use the Gauss-Laguerre integration method for the calculation of the integral,

$$\int_{E_{min}}^{\infty} f_{Mw}(E)v(E)\sigma(E)\,dE, \tag{9}$$

we must transform it to the form,

$$\int_{0}^{\infty} g(x)e^{-x}\,dx. \tag{10}$$

Here,

$$f_{Mw} = \frac{2}{\sqrt{\pi}}\frac{E^{1/2}}{(kT_{cold})^{3/2}}e^{-E/kT_{cold}} \tag{11}$$

is the Maxwell distribution function, where E is the kinetic energy of the incident electron, T is the thermodynamical temperature, and k the Boltzmann constant. Using the relativistic form of E, we can write the electron velocity as

$$v = cE^{1/2}\frac{(E+2mc^2)^{1/2}}{(E+mc^2)}, \tag{12}$$

which leads to

$$\int_{E_{min}}^{\infty} f_{Mw}(E)v(E)\sigma(E)\,dE$$
$$= \frac{2c}{\sqrt{\pi}(kT_{cold})^{3/2}}\int_{E_{min}}^{\infty} Ee^{-E/kT_{cold}}\frac{(E+2mc^2)^{1/2}}{(E+mc^2)}\sigma(E)\,dE. \tag{13}$$

By performing the transformation of variables,

$$z = E - E_{min} \rightarrow E = z + E_{min} \rightarrow dE = dz, \tag{14}$$

we arrive, in a straightforward manner, at (cf. Appendix)

$$\int_{E_{min}}^{\infty} f_{Mw}(E)v(E)\sigma(E)\,dE$$
$$= \frac{2c}{\sqrt{\pi}}\frac{e^{-E_{min}/kT_{cold}}}{(kT_{cold})^{1/2}}\int_{0}^{\infty} g(x)e^{-x}\,dx, \tag{15}$$

where

$$g(x) = (xkT_{cold}+E_{min})\frac{(xkT_{cold}+E_{min}+2mc^2)^{1/2}}{(xkT_{cold}+E_{min}+mc^2)}$$
$$\times \sigma(xkT_{cold}+E_{min}). \tag{16}$$

In what concerns the non-Maxwellian electron distribution function, we follow the suggestion of Celata [57] and use the relativistic version of the Dory-Guest-Harris (DGH) expression [13,58],

$$f_{NMw} = C_n E\left(1+\frac{E}{2mc^2}\right)\left(1+\frac{E}{mc^2}\right)e^{-E/kT_{hot}}, \tag{17}$$

where

$$C_n = \frac{1}{(kT_{hot})^2}\frac{1}{1+3\alpha+3\alpha^2}, \tag{18}$$

with

$$\alpha = \frac{(kT_{hot})}{mc^2}. \tag{19}$$

A process similar to the one used for the Maxwellian electron distribution leads to

$$\int_{E_{min}}^{\infty} f_{NMw}(E)v(E)\sigma(E)\,dE$$
$$= \frac{C_n c(kT_{hot})}{2(mc^2)^2}e^{-E_{min}/kT_{hot}}\int_{0}^{\infty} g(x)e^{-x}\,dx, \tag{20}$$

where

$$g(x) = [x(kT_{hot})+E_{min}]^{3/2}[x(kT_{hot})+E_{min}+2mc^2]^{3/2}$$
$$\times \sigma[x(kT_{hot})+E_{min}]. \tag{21}$$

IV. CALCULATION OF LINE INTENSITIES

We will assume that all ions in the charge state q, where q is the degree of ionization ($q = Z - m$, m being the number of bound electrons in the ion), are initially in the ground configuration. Considering the processes leading to an ion in the charge state q with a K hole and in the excited level i, the balance equation can be written as

$$N_0^q\langle N_e v\sigma_i^{K\text{-exc},q}\rangle + N_0^{q-1}\langle N_e v\sigma_i^{K\text{-ion},(q-1,q)}\rangle$$
$$+ N_0^{q-2}\langle N_e v\sigma_i^{K\text{-double-ion},(q-2,q)}\rangle$$
$$+ N_0^{q-3}\langle N_e v\sigma_i^{K\text{-triple-ion},(q-3,q)}\rangle = N_i^{K,q}A_i^q, \tag{22}$$

where A_i^q is the level i decay probability by any process (radiative and radiationless), $N_0^{q'}$ is the q' charge-state ion density in the ground configuration. In the same equation, $\sigma_i^{K\text{-exc},q}$ is the excitation cross section for the processes leading from an ion in the charge state q in the ground configuration to the excited level i of the same ion with a K hole, and $\sigma_i^{K\text{-ion},(q-1,q)}$, $\sigma_i^{K\text{-double-ion},(q-2,q)}$, and $\sigma_i^{K\text{-triple-ion},(q-3,q)}$ are the single-, double-, and triple-ionization cross sections, respectively, leading from the ions with positive charge q' ($q' = q - 3, \ldots, q$), in the ground configuration, to the excited level i of the ion with charge q and a K hole. $N_i^{K,q}$ is the density of ions in the charge state q, with a K-shell hole and in the level i. The quantities $\langle N_e v\sigma\rangle$ for each process are calculated using Eq. (8).

The $\sigma_i^{K\text{-exc},q}$ values are obtained by summing the individual cross sections σ_{ji} for the processes leading from each level j of the X^{q+} ion ground configuration, to the excited level i of the X^{q+} ion with a K-shell hole, weighted by the statistical weight g_j of each j level of the ground configuration.

In what concerns ionization, the cross section, leading from the $X^{(q-n)+}$ ($n = 1,2,3$) ion in the ground configuration to the X^{q+} ion with a K hole, given by Eqs. (5) and (6), are multiplied by the statistical weight g_i of the level i, yielding the K-shell ionization cross sections $\sigma_i^{K\text{-ion},(q-n,q)}$.
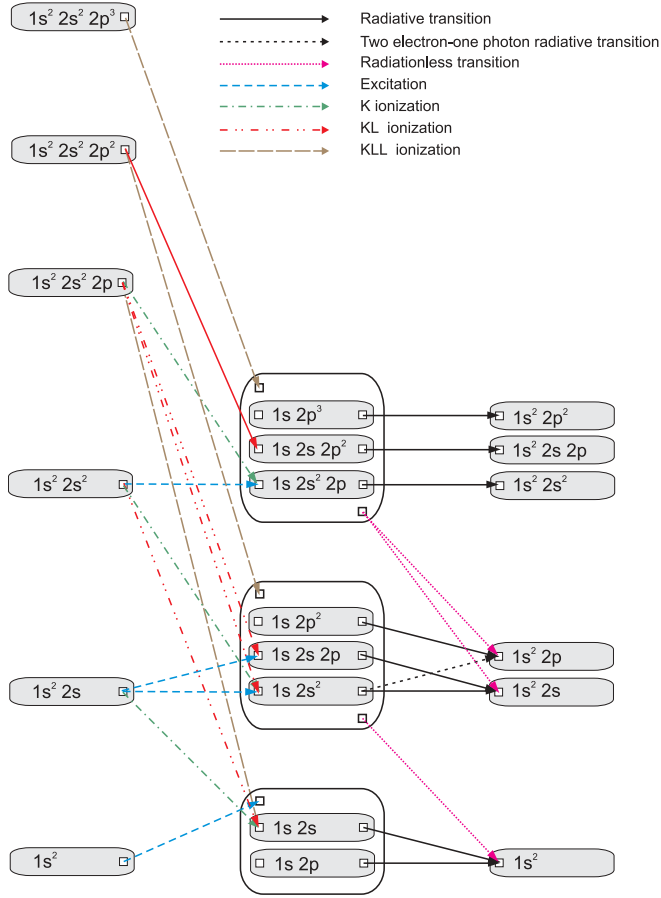
FIG. 3. (Color online) Excitation, ionization, and decay processes considered in this model: *K* excitation, dashed line; single *K* ionization, dot-dashed line; double *KL* ionization, dot-dot-dashed line; triple *KLL* ionization, dot-dot-dot-dash-dashed line; radiative decay, solid line, and radiationless decay, dotted line.

The intensity of the line corresponding to the transition of an ion with charge q and a K-shell hole from the level i to the level j is given by

$$I_{ij}^q = \hbar\omega A_{ij}^q N_i^{K,q}, \qquad (23)$$

where $\hbar\omega$ is the transition energy, A_{ij}^q is the probability of the $i \rightarrow j$ radiative transition, and $N_i^{K,q}$ is obtained from Eq. (22).

All possible excitation, mono-, double-, and triple-ionization processes leading, from the ground configuration of ions with two to seven electrons to excited states of ions with two to four electrons, with a K hole, as well as the de-excitation processes of the latter ones, are illustrated schematically in Fig. 3.

V. APPLICATION TO A SULFUR PLASMA

The method outlined earlier has been applied to the analysis of high-resolution sulfur x-ray spectra obtained in the PSI ECRIT [59], by the Pionic Hydrogen Collaboration [60]. The experimental setup was composed mainly of two parts: an ECR ion trap [11] and a Bragg spectrometer setup in Johann geometry [61,62]. The x rays reflected by the spectrometer crystal were recorded by a two-dimensional CCD

camera [63] placed in the proximity of the Rowland circle of the spectrometer. Details about calibration and spectra construction can be found in Refs. [59,64].

The spectra obtained at PSI cover the 2.400–2.460-keV energy range. The more important features in these spectra are the He-like $1s2s\,^3S_1 \rightarrow 1s^2\,^1S_0$ M1 line at 2.430 keV, and the Li-like $1s2s2p\,^2P_J \rightarrow 1s^22s\,^2S_{1/2}$, $J = 1/2,3/2$ lines, at 2.437 and 2.438 keV, respectively.

The general relativistic MDFGME code developed by Desclaux and Indelicato [32–34], which includes QED corrections, was used to calculate bound-state wave functions and energies, ionization energies, and radiative and radiationless transition probabilities. Details of the MCDF method, including the Hamiltonian and the processes used to build the MCDF wave functions can be found elsewhere [65,66]. In what concerns the QED treatment, the one-electron self-energy is evaluated using the one-electron values of Mohr and co-workers [67–69], and the self-energy screening is treated with the Welton method developed in Refs. [33,70–72]. The vacuum polarization is calculated as described in Ref. [73]. The Uelhing contribution is evaluated to all orders by being included in the self-consistent field (SCF). The Wichmann and Kroll, and Källén and Sabry contributions are included perturbatively. These three contributions are evaluated using the numerical procedure from Refs. [74,75].

An enlarged basis space was used, including all possible electron configurations built from orbitals in the $n = 1, 2, 3$, and 4 electronic shells, corresponding to single and double excitations from the main configuration [76].

To calculate the $\langle N_e \sigma v \rangle$ for each process, given by Eq. (8), we considered $kT_{\text{cold}} = 1$ keV, $kT_{\text{hot}} = 20$ keV, and the value $x = 0.1$. The choice of these temperature values was guided by a survey of temperature measurements from the electrons in the plasma of a variety of ECRIS [5,11,56,77–80], with both smaller and higher microwave frequency (2.45–28 GHz) and a large variety of mirror ratios (2.4–11) for the source considered here, with conventional, permanent, or superconducting magnets.

The quality of the agreement between the simulated and experimental spectra was also taken into account. Furthermore, we also performed the calculations for a hot electron energy of $kT = 30$ keV and we did not found significant differences in the spectra. The weak influence of the hot electron energy kT is probably due to the strong decrease of the ionization cross section with electron energy. Recent works have demonstrated improved performances in source with higher magnetic-field gradients (corresponding to increased magnetic mirror ratios) [81,82] concomitant with a reduction of the hot electron density and radiations. The good performances of the ECRIT for production of x rays of highly charged ions, with its very large mirror ratio seems to confirm these results. Only a direct measurement, yet to be performed (e.g., by a study of the bremsstrahlung spectrum), will provide a quantitative answer.

The calculated spectrum (normalized to the 2438-eV peak intensity) obtained using the method discussed earlier and assuming, for each line, a linear combination of a Gaussian and a Lorentzian distribution, designed to approximate a Voigt profile with a total width of 0.3 eV, is presented in Fig. 4 in a semilogarithmic scale (a), and in a linear scale (b). From
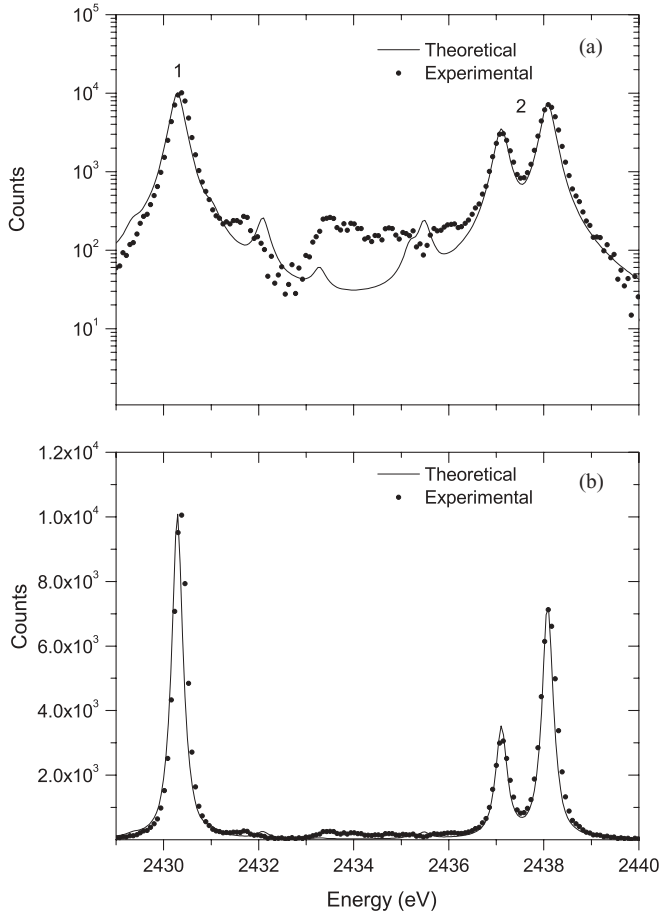
FIG. 4. Theoretical spectra of a sulfur plasma (solid curve) plotted against experimental data (dots) in log scale (a) and linear scale (b). Peak 1 refers to the M1 $1s\,2s\,^3S_1 \rightarrow 1s^2$ line, and peak 2 to the $1s\,2s\,2p\,^2P_{1/2,3/2} \rightarrow 1s2\,2s$ lines and to the $1s\,2p\,^3P_1 \rightarrow 1s^2$ line. The experimental data were obtained in the PSI ECRIT [11].

the comparison with experiment we note that, although the most intense peaks are well reproduced, there are several weak features above statistical noise, which are not reproduced. Some of them could be due to $n = 3$ or 4 satellite lines of the heliumlike and lithiumlike ions. Yet our calculations and a search in x-ray transition energy database [83] did not reveal lines that could explain those features.

In Table I we list the ion charge-state density ratios obtained from the comparison of the peak intensities in theoretical and experimental spectra.

TABLE I. Ion charge-state density ratios S^{q+}/S^{14+} obtained from the comparison of the peak intensities in theoretical and experimental spectra measured in the PSI ECRIT [11].

	Ion density ratios
S^{9+}/S^{14+}	50
S^{10+}/S^{14+}	63
S^{11+}/S^{14+}	63
S^{12+}/S^{14+}	59
S^{13+}/S^{14+}	18

VI. CONCLUSIONS

In this work, we have presented a method to estimate the ion CSD in an ECRIS through the analysis of the x-ray spectra emitted by the plasma. This method is an improvement of the method described in Ref. [22], that takes into account a more realistic electron energy distribution and the triple ionization by electron impact.

The proposed method has been applied to the analysis of an ECRIS sulfur plasma x-ray spectrum to obtain ion densities. The calculated spectrum reproduces quite well the most intense peaks.

APPENDIX: GAUSS-LAGUERRE INTEGRATION

We will use the Gauss-Laguerre integral form [84],

$$\int_0^\infty e^{-x} f(x)\, dx \approx \sum_{i=1}^n w_i f(x_i), \tag{A1}$$

where x_i is the ith root of the Laguerre polynomial $L_n(x)$, and the weight w_i is given by

$$w_i = \frac{x_i}{(n+1)^2[L_{n+1}(x_i)]^2}. \tag{A2}$$

1. Maxwell distribution

We want to write the integral,

$$\int_{E_{\min}}^\infty f_{\text{Mw}}(E) v(E) \sigma(E)\, dE, \tag{A3}$$

in the form,

$$\int_0^\infty g(x) e^{-x}\, dx, \tag{A4}$$

in order to apply the Gauss-Laguerre integration method. Replacing the Maxwell distribution function,

$$f_{\text{Mw}} = \frac{2}{\sqrt{\pi}} \frac{E^{1/2}}{(kT_{\text{cold}})^{3/2}} e^{-E/kT_{\text{cold}}}, \tag{A5}$$

in Eq. (A3), we get

$$\int_{E_{\min}}^\infty f_{\text{Mw}}(E) v(E) \sigma(E)\, dE$$
$$= \frac{2c}{\sqrt{\pi}(KT_{\text{cold}})^{3/2}} \int_{E_{\min}}^\infty E e^{-E/kT_{\text{cold}}} \frac{(E+2mc^2)^{1/2}}{(E+mc^2)} \sigma(E)\, dE. \tag{A6}$$

Considering that

$$z = E - E_{\min} \rightarrow E = z + E_{\min}, \quad \text{(A7)}$$

Eq. (A6) reads

$$\int_{E_{\min}}^{\infty} f_{\mathrm{Mw}}(E)v(E)\sigma(E)\,dE$$
$$= \frac{2ce^{-E_{\min}/kT_{\mathrm{cold}}}}{\sqrt{\pi}(kT_{\mathrm{cold}})^{3/2}} \int_0^{\infty} (z + E_{\min})e^{-z/kT_{\mathrm{cold}}}$$
$$\times \frac{(z + E_{\min} + 2mc^2)^{1/2}}{(z + E_{\min} + mc^2)}\sigma(z + E_{\min})\,dz. \quad \text{(A8)}$$

Performing the variable change,

$$x = \frac{z}{kT_{\mathrm{cold}}} \rightarrow z = xkT_{\mathrm{cold}} \rightarrow dz = kT_{\mathrm{cold}}\,dx, \quad \text{(A9)}$$

Eq. (A8) assumes the form,

$$\int_{E_{\min}}^{\infty} f_{\mathrm{Mw}}(E)v(E)\sigma(E)\,dE$$
$$= \frac{2c}{\sqrt{\pi}} \frac{e^{-E_{\min}/kT_{\mathrm{cold}}}}{(kT_{\mathrm{cold}})^{1/2}} \int_0^{\infty} g(x)e^{-x}\,dx, \quad \text{(A10)}$$

where

$$g(x) = (xkT_{\mathrm{cold}} + E_{\min})\frac{(xkT_{\mathrm{cold}} + E_{\min} + 2mc^2)^{1/2}}{(xkT_{\mathrm{cold}} + E_{\min} + mc^2)}$$
$$\times \sigma(xkT_{\mathrm{cold}} + E_{\min}). \quad \text{(A11)}$$

2. Non-Maxwell distribution

Following the same reasoning for the non-Maxwellian distribution f_{NMw}, the integral,

$$\int_{E_{\min}}^{\infty} f_{\mathrm{NMw}}(E)v(E)\sigma(E)\,dE, \quad \text{(A12)}$$

with

$$f_{\mathrm{NMw}} = C_n E\left(1 + \frac{E}{2mc^2}\right)\left(1 + \frac{E}{mc^2}\right)e^{-E/kT_{\mathrm{hot}}}, \quad \text{(A13)}$$

where

$$C_n = \frac{1}{(kT_{\mathrm{hot}})^2}\frac{1}{1 + 3\alpha + 3\alpha^2} \quad \text{and} \quad \alpha = \frac{(kT_{\mathrm{hot}})}{mc^2}, \quad \text{(A14)}$$

is given by

$$\int_{E_{\min}}^{\infty} f_{\mathrm{NMw}}(E)v(E)\sigma(E)\,dE$$
$$= \frac{C_n c}{2(mc^2)^2} \int_{E_{\min}}^{\infty} E^{3/2}(E + 2mc^2)^{3/2}e^{-E/kT_{\mathrm{hot}}}\sigma(E)\,dE. \quad \text{(A15)}$$

Considering that

$$z = E - E_{\min} \rightarrow E = z + E_{\min} \rightarrow dE = dz, \quad \text{(A16)}$$

Eq. (A15) assumes the form,

$$\int_{E_{\min}}^{\infty} f_{\mathrm{NMw}}(E)v(E)\sigma(E)\,dE$$
$$= \frac{C_n c e^{-E_{\min}/kT_{\mathrm{hot}}}}{2(mc^2)^2} \int_{E_{\min}}^{\infty} (z + E_{\min})^{3/2}$$
$$\times (z + E_{\min} + 2mc^2)^{3/2}e^{-z/kT_{\mathrm{hot}}}\sigma(z + E_{\min})\,dz. \quad \text{(A17)}$$

Performing the variable change,

$$x = \frac{z}{(kT_{\mathrm{hot}})} \rightarrow z = x(kT_{\mathrm{hot}}) \rightarrow dz = (kT_{\mathrm{hot}})\,dx, \quad \text{(A18)}$$

we transform Eq. (A17) in the form,

$$\int_{E_{\min}}^{\infty} f_{\mathrm{NMw}}(E)v(E)\sigma(E)\,dE$$
$$= \frac{C_n c(kT_{\mathrm{hot}})e^{-E_{\min}/kT_{\mathrm{hot}}}}{2(mc^2)^2} \int_{E_{\min}}^{\infty} g(x)e^{-x}\,dx, \quad \text{(A19)}$$

with

$$g(x) = [x(kT_{\mathrm{hot}}) + E_{\min}]^{3/2}[x(kT_{\mathrm{hot}}) + E_{\min} + 2mc^2]^{3/2}$$
$$\times c\sigma[x(kT_{\mathrm{hot}}) + E_{\min}]. \quad \text{(A20)}$$

[1] P. Grübling, J. Hollandt, and G. Ulm, Rev. Sci. Instrum. **71**, 1200 (2000).

[2] M. Trassinelli *et al.*, J. Phys.: Conference Series **58**, 129 (2007).

[3] E. O. Le Bigot *et al.*, Phys. Scr. T **134**, 014015 (2009).

[4] G. Douysset, H. Khodja, A. Girard, and J. P. Briand, Phys. Rev. E **61**, 3015 (2000).

[5] A. Gumberidze *et al.*, Rev. Sci. Instrum. **81**, 033303 (2010).

[6] D. F. Anagnostopoulos *et al.*, Nucl. Instrum. Methods Phys. Res., Sect. A **545**, 217 (2005).

[7] R. Geller, *Electron Cyclotron Resonance Ion Sources and ECR Plasmas* (Institute of Physics Publishing, Bristol, 1996).

[8] D. Leitner, C. M. Lyneis, S. R. Abbott, D. Collins, R. D. Dwinell, M. L. Galloway, M. Leitner, and D. S. Todd, Nucl. Instrum. Meth. B **235**, 486 (2005).

[9] P. Ludwig *et al.*, Rev. Sci. Instrum. **69**, 4082 (1998).

[10] S. Gammino, G. Ciavola, L. Celona, D. Hitz, A. Girard, and G. Melin, Rev. Sci. Instrum. **72**, 4090 (2001).

[11] S. Biri, L. Simons, and D. Hitz, Rev. Sci. Instrum. **71**, 1116 (2000).

[12] G. Melin, Int. J. Mass Spectrom. **192**, 87 (1999).

[13] C. Barué, M. Lamoureux, P. Briand, A. Girard, and G. Melin, J. Appl. Phys. **76**, 2662 (1994).

[14] G. Melin, A. G. Drentje, A. Girard, and D. Hitz, J. Appl. Phys. **86**, 4772 (1999).

[15] A. G. Drentje, Rev. Sci. Instrum. **74**, 2631 (2003).

[16] R. Friedlein, S. Heprich, U. Lehnert, H. Tyrroff, H. Wirth, C. Zippe, and G. Zschornack, Nucl. Instrum. Meth. Phys. B **98**, 585 (1995).

[17] U. Lehnert, C. Zippe, and G. Zschornack, Hyperfine Interact. **99**, 235 (1996).

[18] C. Heinzelmann, U. Lehnert, D. Küchler, and G. Zschornack, Hyperfine Interact. **108**, 51 (1997).

[19] P. Grübling, D. Küchler, U. Lehnert, A. Ullrich, T. Werner, and G. Zschornack, Rev. Sci. Instrum. **69**, 1167 (1998).

[20] D. Küchler, F. Ullmann, T. Werner, G. Zschornack, H. Tyrroff, and P. Grübling, Nucl. Instr. Meth. Phys. Res. B **168**, 566 (2000).

[21] J. B. Boffard *et al.*, J. Phys. D **37**, R143 (2004).

[22] M. C. Martins, A. M. Costa, J. P. Santos, P. Indelicato, and F. Parente, J. Phys. B **34**, 533 (2001).

[23] J. P. Marques, F. Parente, and P. Indelicato, Phys. Rev. A **47**, 929 (1993).

[24] T. Brage, P. G. Judge, A. Aboussaid, M. R. Godefroid, P. Joensson, A. Ynnerman, C. Froese Fischer, and D. S. Leckrone, Astrophys. J. **500**, 507 (1998).

[25] J. P. Marques, F. Parente, and P. Indelicato, At. Data Nucl. Data Tables **55**, 157 (1993).

[26] S. G. Porsev and A. Derevianko, Phys. Rev. A **69**, 042506 (2004).

[27] Y.-K. Kim, K. K. Irikura, M. E. Rudd, M. A. Ali, and P. M. Stone, Electron-impact cross sections for ionization and excitation [http://physics.nist.gov/ionxsec] (2009).

[28] Plasma Laboratory of Weizmann Institute of Science, Databases for atomic and plasma physics [http://plasma-gate.weizmann.ac.il/DBfAPP.html] (2003).

[29] V. Fisher, V. Bernshtam, H. Golten, and Y. Maron, Phys. Rev. A **53**, 2425 (1996).

[30] H. van Regemorter, Astrophys. J. **136**, 906 (1962).

[31] Plasma Laboratory of Weizmann Institute of Science, Free software for atomic and plasma physics [http://plasma-gate.weizmann.ac.il/DBfAPP.html] (2003).

[32] J. P. Desclaux, Comput. Phys. Commun. **9**, 31 (1975).

[33] P. Indelicato and J. P. Desclaux, Phys. Rev. A **42**, 5139 (1990).

[34] P. Indelicato and J. Desclaux, computer program MCDFGME, a multiconfiguration Dirac-Fock and general matrix elements program (release 2005) [http://dirac.spectro.jussieu.fr/mcdf].

[35] Y.-K. Kim and K.-T. Cheng, Phys. Rev. A **18**, 36 (1978).

[36] J. P. Santos and F. Parente, Eur. Phys. J. D—At. Molec. Opt. Plasma Phys. **47**, 339 (2008).

[37] P. G. Burke and K. A. Berrington, *Atomic and Molecular Processes: An R-Matrix Approach* (Institute of Physics, New York, 1993).

[38] I. Bray and A. T. Stelbovics, Comput. Phys. Commun. **85**, 1 (1995).

[39] F. Robicheaux, M. S. Pindzola, and D. R. Plante, Phys. Rev. A **55**, 3573 (1997).

[40] M. Baertschy, T. N. Rescigno, and C. W. McCurdy, Phys. Rev. A **64**, 022709 (2001).

[41] P. L. Bartlett and A. T. Stelbovics, Phys. Rev. A **66**, 012707 (2002).

[42] K. N. Joshipura, S. Gangopadhyay, and B. G. Vaishnav, J. Phys. B: At. Molec. Opt. Phys. **40**, 199 (2007).

[43] J. Berakdar, A. Lahmam-Bennani, and C. D. Cappello, Phys. Rep. **374**, 91 (2003).

[44] W. Lotz, Z. Phys. A **216**, 241 (1968).

[45] H. Deutsch, K. Becker, and T. D. Mark, Int. J. Mass Spectrom. Ion Processes **177**, 47 (1998).

[46] E. Casnati, A. Tartari, and C. Baraldi, J. Phys. B: At. Molec. Phys. **15**, 155 (1982).

[47] C. A. Quarles, Phys. Rev. A **13**, 1278 (1976).

[48] Y.-K. Kim and M. E. Rudd, Phys. Rev. A **50**, 3954 (1994).

[49] Y.-K. Kim and P. M. Stone, Phys. Rev. A **64**, 052707 (2001).

[50] Y.-K. Kim and J.-P. Desclaux, Phys. Rev. A **66**, 012708 (2002).

[51] Y.-K. Kim, J. P. Santos, and F. Parente, Phys. Rev. A **62**, 052710 (2000).

[52] J. P. Santos, F. Parente, and Y.-K. Kim, J. Phys. B **36**, 4211 (2003).

[53] D. Berenyi, G. Hock, S. Ricz, B. Schlenk, and A. Valek, J. Phys. B: At. Molec. Phys. **11**, 709 (1978).

[54] V. P. Shevelko and H. Tawara, J. Phys. B **28**, L589 (1995).

[55] C. Bélenger, P. Defrance, E. Salzborn, V. P. Shevelko, H. Tawara, and D. B. Uskov, J. Phys. B **30**, 2667 (1997).

[56] R. Pras, M. Lamoureux, A. Girard, H. Khodja, and G. Melin, Rev. Sci. Instrum. **69**, 700 (1998).

[57] C. M. Celata, Nucl. Fusion **25**, 35 (1985).

[58] R. A. Dory, G. E. Guest, and E. G. Harris, Phys. Rev. Lett. **14**, 131 (1965).

[59] M. Trassinelli, Ph.D. thesis, P. et M. Curie, Paris, 2005.

[60] Pionic Hydrogen Collaboration [http://www.fz-juelich.de/ikp/exotic-atoms/index.php] (2003).

[61] D. Gotta *et al.* , Nucl. Phys. A **660**, 283 (1999).

[62] D. F. Anagnostopoulos *et al.*, Nucl. Instrum. Meth. Phys. A **545**, 217 (2005).

[63] N. Nelms *et al.*, Nucl. Instrum. Meth. Phys. A **484**, 419 (2002).

[64] P. Indelicato, M. Trassinelli, D. F. Anagnostopoulos, S. Boucard, D. S. Covita, G. Borchert, A. Dax, J. P. Egger, D. Gotta, and A. Gruber, *Advances in Quantum Chemistry* (Academic Press, San Diego, 2007).

[65] I. P. Grant and H. M. Quiney, Adv. At. Mol. Phys. **23**, 37 (1988).

[66] P. Indelicato, Phys. Rev. A **51**, 1132 (1995).

[67] P. J. Mohr, Phys. Rev. A **26**, 2338 (1982).

[68] P. J. Mohr and Y.-K. Kim, Phys. Rev. A **45**, 2727 (1992).

[69] P. J. Mohr, Phys. Rev. A **46**, 4421 (1992).

[70] P. Indelicato, O. Gorceix, and J. P. Desclaux, J. Phys. B **20**, 651 (1987).

[71] P. Indelicato and E. Lindroth, Phys. Rev. A **46**, 2426 (1992).

[72] P. Indelicato, S. Boucard, and E. Lindroth, Eur. Phys. J. D **3**, 29 (1998).

[73] S. Boucard and P. Indelicato, Eur. Phys. J. D **8**, 59 (2000).

[74] S. Klarsfeld, Phys. Lett. A **30**, 382 (1969).

[75] L. W. Fullerton and J. G. A. Rinkler, Phys. Rev. A **13**, 1283 (1976).

[76] M. C. Martins, J. P. Marques, A. M. Costa, J. P. Santos, F. Parente, S. Schlesser, E.-O. LeBigot, and P. Indelicato, Phys. Rev. A **80**, 032501 (2009).

[77] C. Baru, M. Lamoureux, P. Briand, A. Girard, and G. Melin, J. Appl. Phys. **76**, 2662 (1994).

[78] M. Bacal, C. Gaudin, A. Bourdier, J. Bruneteau, J. M. Buzzi, K. S. Golovanivsky, L. Hay, C. Rouill, and L. Schwartz, Nature (London) **384**, 421 (1996).

[79] C. Gaudin, L. Hay, J. M. Buzzi, M. Bacal, and M. Lamoureux, Rev. Sci. Instrum. **69**, 890 (1998).

[80] D. Leitner, J. Y. Benitez, C. M. Lyneis, D. S. Todd, T. Ropponen, J. Ropponen, H. Koivisto, and S. Gammino, Rev. Sci. Instrum. **79**, 033302 (2008).

[81] S. Gammino, D. Mascali, L. Celona, F. Maimone, and G. Ciavola, Plasma Sources Sci. Technol. **18**, 045016 (2009).

[82] D. Leitner, C. M. Lyneis, T. Loew, D. S. Todd, S. Virostek, and O. Tarvainen, Rev. Sci. Instrum. **77**, 03A302 (2006).

[83] R. D. Deslattes, E. G. Kessler, P. Indelicato, L. de Billy, E. Lindroth, and J. Anton, Rev. Mod. Phys. **75**, 35 (2003).

[84] M. Abramowitz and I. A. Stegun, *Handbook of Mathematical Functions*, 10th ed. (Dover Publications, New York, 1972).

[85] H. Tawara, K. G. Harrison, and F. J. D. Heer, Physica **63**, 351 (1973).

[86] R. Hippler, K. Saeed, I. McGregor, and H. Kleinpoppen, Z. Phys. A **307**, 83 (1982).

[87] C. Quarles and M. Semaan, Phys. Rev. A **26**, 3147 (1982).

[88] H. Platten, G. Schiwietz, and G. Nolte, Phys. Lett. A **107**, 89 (1985).

[89] W. Lotz, Z. Phys. A **206**, 205 (1967).

[90] W. Scholz, A. Li-Scholz, R. Coll, and I. L. Preiss, Phys. Rev. Lett. **29**, 761 (1972).

[91] K. Kiss, G. Kálmán, J. Pálinkás, and B. Schlenk, Acta Physica Hungarica **50**, 97 (1981).